Hybrid RSM–ANN–GA Optimization of TIG Hot-Wire Welding for AISI 5160 Steel

Phattharapong Keidlaphi
Department of Manufacturing Engineering, Faculty of Engineering and Architecture, Rajamangala University of Technology Suvarnabhumi, Phra Nakhon Si Ayutthaya, Thailand
pongsak.ke@rmutsb.ac.th

Sittichai Charonerat
Department of Industrial Technology, Nakhon Phanom University, Nakhon Phanom, Thailand
akecharone@npu.ac.th

Suriya Prasomthong
Department of Industrial Technology, Nakhon Phanom University, Nakhon Phanom, Thailand
suriya.p@npu.ac.th

Teephet Chaiyason
Department of Industrial Technology, Nakhon Phanom University, Nakhon Phanom, Thailand
teepach20@npu.ac.th (corresponding author)

Received: 29 January 2026 | Revised: 8 March 2026 | Accepted: 15 March 2026

 DOI: https://doi.org/10.48084/etasr.17832

ABSTRACT

Repair welding of AISI 5160 chromium spring steel is challenging due to its high sensitivity to thermal cycling, which may cause HAZ softening, carbide instability, and reduced toughness. This study proposes an integrated Response Surface Methodology–Artificial Neural Network–Genetic Algorithm (RSM–ANN–GA) framework for predicting and optimizing the multi-objective performance of TIG hot-wire repair welding, aiming to simultaneously enhance weld hardness and impact energy under limited experimental data. A compact Central Composite Design (CCD) with nine runs was employed, by varying Welding Current (WC) and Hot-Wire Current (HWC), while travel speed was kept constant. The measured responses ranged from 49.6–62.2 HRC and 19.8–35.5 J, indicating a strength–toughness interaction governed by heat-balance control. Quadratic RSM–CCD models assessed by ANOVA showed excellent adequacy for hardness (R^2 = 0.979; Adjusted R^2 = 0.944), dominated by WC and WC² effects, whereas impact energy was primarily influenced by nonlinear HWC terms with moderate predictability (R^2 = 0.882; Adjusted R^2 = 0.686). A feed-forward ANN (2–10–2) provided higher predictive accuracy (R^2 = 0.97 for hardness; R^2 = 0.99 for impact energy) compared to RSM. ANN was embedded into a desirability-based GA optimizer, yielding an optimal condition at WC = 200 A and HWC = 150 A, with predicted responses of 58.17 HRC and 35.55 J, with a high desirability (*D*) of 0.95. Microstructural and fractographic results supported enhanced weld uniformity and ductile fracture behavior.

Keywords-TIG hot-wire welding; RSM–CCD; artificial neural network; genetic algorithm optimization

I. INTRODUCTION

AISI 5160 chromium spring steel is extensively used in automotive and heavy-duty industrial components because its medium-carbon chemistry and Cr-assisted carbide strengthening provide high toughness, fatigue resistance, and wear durability under cyclic and abrasive service conditions [1]. Despite its excellent hardenability and ability to achieve martensitic hardness exceeding 60 HRC after quenching [2], AISI 5160 is highly sensitive to welding thermal cycles. Inadequate heat control during repair welding can induce HAZ softening, local embrittlement, and degradation of the hardness–toughness balance due to over-tempering and carbide coarsening [3]. Given that service failures of AISI 5160 components frequently involve fatigue or impact loading [4], reliable and cost-effective repair welding is crucial for extending service life.

Gas Tungsten Arc Welding (GTAW/TIG) is widely used in industrial welding and repair applications due to its excellent arc stability and precise heat input control [5, 6]; however, conventional cold-wire TIG welding may still impose

unfavorable thermal histories in high-strength steels, leading to strength–toughness trade-offs governed by heat input and cooling trajectories [6]. TIG hot-wire welding has therefore attracted attention as an advanced repair technique, wherein the filler wire is independently preheated to enhance melting efficiency, stabilize deposition, and reduce effective heat transfer to the base metal, thereby limiting excessive HAZ growth and improving metallurgical stability. Nevertheless, the process response is governed by strongly nonlinear interactions among Welding Current (WC), Hot-Wire Current (HWC), and thermal balance, which directly control phase transformations, alloy dilution, and fracture-related properties.

As a result, empirical parameter selection is inefficient for achieving simultaneous optimization of hardness and impact toughness. While Response Surface Methodology (RSM) combined with Central Composite Design (CCD) is used to model nonlinear welding responses with limited experiments, quadratic models may show limited predictive fidelity for fracture-sensitive properties under small datasets [7]. Artificial Neural Networks (ANN) offer superior capability for capturing complex mechanical property interactions [8], whereas Genetic Algorithms (GA) enable efficient global optimization of multi-objective response spaces and are particularly effective when coupled with desirability-based formulations [9]. The proposed in [10] hybrid Response Surface Methodology–Artificial Neural Network–Genetic Algorithm (RSM–ANN–GA) framework outperformed single-method approaches in multi-response welding optimization problems. However, such an integrated methodology has not been systematically applied to TIG hot-wire repair welding of AISI 5160.

To address this gap, the present study proposes a hybrid RSM–CCD+ANN–GA framework for multi-response optimization of TIG hot-wire repair welding of AISI 5160 to maximize hardness and impact toughness under limited experimental data while ensuring microstructural integrity.

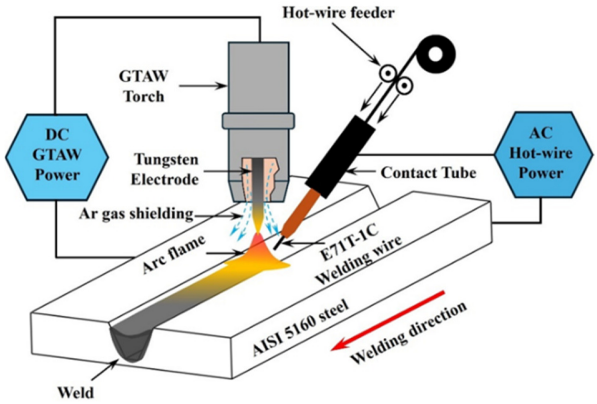

Fig. 1. TIG hot-wire welding setup for AISI 5160 steel.

II. EXPERIMENTAL METHOD

A. Materials, Welding Procedure, and Mechanical Testing

TIG hot-wire repair welding experiments were conducted on AISI 5160 chromium spring steel to generate experimental data for subsequent modeling and optimization. Plates with dimensions of 100 mm × 150 mm × 16 mm were prepared, and a single-V groove with a 60° included angle was machined in accordance with AWS D1.1/D1.1M to ensure consistent joint geometry. A schematic of the TIG hot-wire welding configuration is shown in Figure 1.

The chemical compositions of AISI 5160 and the E71T-1C filler wire are listed in Table I. A 1.2 mm filler wire was selected for compatibility with medium-carbon alloy steels. Welding was conducted using an automated TIG hot-wire system with 99.99% argon shielding, where the filler wire was independently preheated to enhance melting efficiency and control effective heat input.

TABLE I. CHEMICAL COMPOSITION OF BASE METALS AND FILLER

Material	C	Mn	Si	P	S	Cr	Ni	Fe
AISI5160	0.58	0.81	0.27	0.028	0.032	0.76	0.41	Bal.
E71T-1C	0.12	1.24	0.46	0.021	0.024	-	0.22	Bal.

WC and HWC were varied, whereas travel speed was fixed at 100 mm/min. Post-weld quenching and annealing were applied to simulate the service conditions of AISI 5160. Mechanical performance was assessed via hardness and Charpy U-notch impact energy in accordance with ASTM E23. The hardness was measured across the weld metal and HAZ, as depicted in Figure 2. Macro and microstructural analyses were also performed to evaluate weld integrity and microstructural evolution.

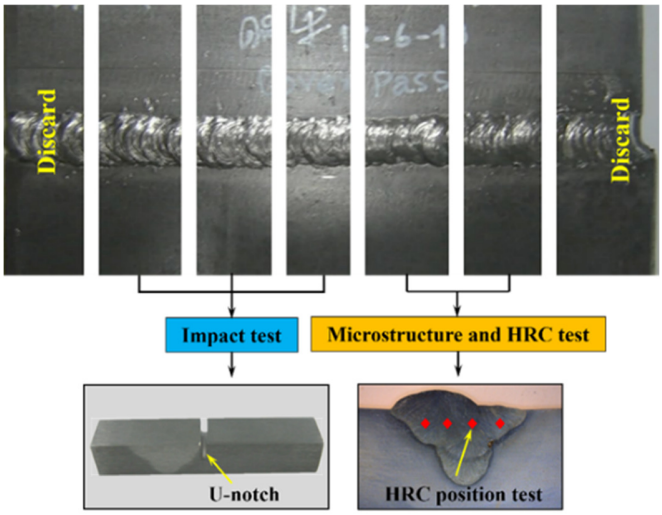

Fig. 2. Specimen preparation and test locations.

B. Experimental Design Using RSM

RSM–CCD was applied to evaluate the effects of WC and HWC on the hardness and impact energy of TIG hot-wire welds with minimal experiments. Two variables were defined at five coded levels (±1, ±α, and center), as presented in Table II, while travel speed was kept constant to isolate electrical effects. To minimize experimental cost and time, a single center point was employed, yielding a nine-run CCD

comprising four factorial, four axial, and one center-point experiments. Hardness and impact energy were measured as responses. The mechanical responses were measured in terms of hardness (HRC) and Charpy impact energy (J) of the welded joints, which were selected as key indicators of the strength–toughness balance of AISI 5160 repair welds. Despite limited estimation of pure error, the design adequately covers the parameter space for trend analysis and surrogate modeling. Based on this dataset, second-order polynomial models were formulated as:

$$Y = \beta_0 + \beta_1 WC + \beta_2 HWC + \beta_{11} WC^2 + \beta_{22} HWC^2 + \beta_{12} WC \cdot HWC \quad (1)$$

where Y denotes the predicted response (hardness or impact energy) and β terms are regression coefficients obtained by least-squares estimation.

Although the quadratic RSM models capture main, interaction, and nonlinear effects, their predictive accuracy is limited by the small dataset and the strong nonlinearity of impact energy. Therefore, the RSM–CCD data were used to train an ANN and coupled with a GA to enhance prediction and enable multi-objective optimization.

TABLE II. PROCESS PARAMETERS AND CODED LEVELS FOR RSM

Factor	Parameter			
	Low	High	- alpha	+ alpha
WC (A)	175	225	164.65	235.35
HWC (A)	120	180	107.57	192.43

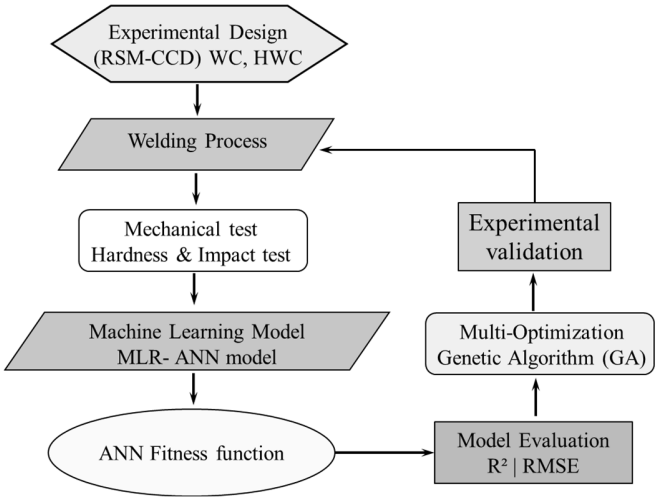

Fig. 3. Hybrid RSM–ANN–GA optimization framework.

C. Prediction and Optimization Framework

An integrated ANN–GA framework was employed to predict mechanical responses and identify optimal welding parameters. The workflow comprising experimental design, ANN modeling, GA-based optimization, and validation is displayed in Figure 3, with the ANN serving as a surrogate model embedded in the GA fitness function. Equations (2) and (3) define the normalization and denormalization of inputs and outputs for ANN modeling. Equations (4) and (5) describe the hidden-layer activation and output formulation of the feed-forward ANN, while (6) gives the Levenberg–Marquardt update rule for efficient training. Equations (7) and (8) formulate the desirability-based objective function, transforming ANN predictions into individual desirabilities and combining them into a single metric for GA-based optimization:

$$x_i^{norm} = 2\left(\frac{x_i - x_i^{norm}}{x_i^{max} - x_i^{min}}\right) - 1,\ i = 1,2 \quad (2)$$

$$y_k = \left(\frac{y_k^{norm}+1}{2}\right)\left(y_k^{max} - y_k^{min}\right) + y_k^{min}, k = 1,2 \quad (3)$$

$$h_j = tanh\left(\sum_{i=1}^{2} w_{ij}\, x_i^{norm} + b_j\right), j = 1,2, \ldots .10 \quad (4)$$

$$y_k^{norm} = \sum_{j=1}^{10} v_{ik} h_j + c_k,\ k = 1,2 \quad (5)$$

$$\theta_{t+1} = \theta_t - (J^T J + \mu I)^{-1} J^T e \quad (6)$$

$$d_r = \begin{cases} 0, & y_r < L_r \\ \left(\dfrac{y_r - L_r}{U_r - L_r}\right)^{w_r}, & L_r \le y_r \le U_r \\ 0, & y_r < L_r \end{cases} \quad (7)$$

$$D = \left(\prod_{r=1}^{2} d_r\right)^{1/2} \quad (8)$$

TABLE III. CCD EXPERIMENTAL MATRIX AND RESPONSES

Run	WC	HWC	Hardness (HRC)	Impact energy (J)
1	175	120	50.8	24.5
2	225	120	60.2	19.8
3	175	180	52.6	29.2
4	225	180	61.0	25.6
5	164.65	150	49.6	34.8
6	235.35	150	62.2	28.5
7	200	107.57	56.0	22.0
8	200	192.43	56.8	30.1
9	200	150	58.0	35.5

III. RESULTS

A. Mechanical Properties and RSM–CCD Analysis

Table III presents the CCD matrix and mechanical responses of TIG hot-wire-welded AISI 5160 joints. Hardness ranged from 49.6 to 62.2 HRC and impact energy from 19.8 to 35.5 J, indicating that electrical parameters strongly governed the strength–toughness balance via their combined effect on heat input and microstructural evolution. In hot-wire TIG, resistance preheating of the filler wire enhances deposition efficiency and alters the thermal cycle relative to cold-wire TIG, thereby influencing hardness and toughness.

The hardness increased primarily with WC, reaching its maximum under the high-current axial condition (Run 6: WC = 235.35 A, HWC = 150 A), where the hardness attained 62.2 HRC, whereas HWC enhanced impact energy at fixed WC, consistent with improved heat balance from hot-wire preheating. This trend aligns with the thermal sensitivity of the hardness–toughness trade-off in AISI 5160. ANOVA of the quadratic RSM–CCD models, presented in Table IV, confirmed excellent model adequacy for hardness (S = 0.30, R^2

= 0.979, Adjusted R^2 = 0.944), with WC being the dominant factor (40.07%, p = 0.0048), followed by WC² (25.07%, p = 0.0094), while HWC and HWC² were also significant; the WC × HWC interaction was insignificant (p = 0.194).

TABLE IV. ANOVA: QUADRATIC RSM MODEL FOR HARDNESS

Source	Df	Sum of squares	F-value	P-value	Contribution (%)
WC	1	5.125	57.02	0.0048	40.07
HWC	1	2.078	23.12	0.0171	16.24
WC^2	1	3.207	35.68	0.0094	25.07
HWC^2	1	1.862	20.71	0.0199	14.55
WC×HWC	1	0.25	2.78	0.1940	1.95
Residual	3	0.27	–	–	2.11

S = 0.30; R^2 = 0.979; Adjusted R^2 = 0.944

TABLE V. ANOVA: QUADRATIC RSM MODEL FOR IMPACT ENERGY

Source	Df	Sum of squares	F-value	P-value	Contribution (%)
WC	1	22.928	2.06	0.2466	8.11
HWC	1	104.985	9.44	0.0545	37.13
WC2	1	25.21	2.27	0.2293	8.92
HWC2	1	95.976	8.63	0.0606	33.94
WC×HWC	1	0.303	0.03	0.8795	0.11
Residual	3	33.369	–	–	11.8

S = 3.34; R^2 = 0.882; Adjusted R^2 = 0.686

In Table V, the quadratic model for impact energy shows moderate fit (S = 3.34, R^2 = 0.882, Adjusted R^2 = 0.686), with significant contributions from HWC (37.13%) and HWC² (33.94%), while WC-related terms are minor and statistically insignificant (α = 0.05). The lower adjusted R^2 indicates higher sensitivity to microstructural and fracture variability, highlighting the limited effectiveness of a compact CCD-based quadratic RSM for accurate impact energy prediction.

TABLE VI. PREDICTION ACCURACY OF ANN AND RSM–CCD

Run	Exp. HRC	Exp. impact	RSM HRC	ANN HRC	RSM impact	ANN impact
1	50.80	24.50	51.00	50.78	26.51	24.50
2	60.20	19.80	60.41	60.19	21.67	19.84
3	52.60	29.20	52.43	52.40	31.45	29.54
4	61.00	25.60	60.84	61.00	27.71	25.74
5	49.60	34.80	49.62	49.64	32.67	34.72
6	62.20	28.50	62.23	62.21	26.60	28.40
7	56.00	22.00	55.76	56.02	20.15	22.00
8	56.80	30.10	57.08	56.67	27.92	29.72
9	58.00	35.50	58.02	58.17	35.52	35.55
R2			0.97	0.99	0.86	0.99
RMSE			0.93	0.10	2.32	0.18

Figure 4(a) shows that hardness increases significantly with WC, exhibiting pronounced curvature, consistent with significant WC and WC² effects. Figure 4(b) exhibits a dome-shaped impact-energy surface, with higher values at intermediate settings and reduced toughness at high-WC/low-HWC conditions, in agreement with ANOVA (Table V), indicating HWC-dominated nonlinear control of impact energy.

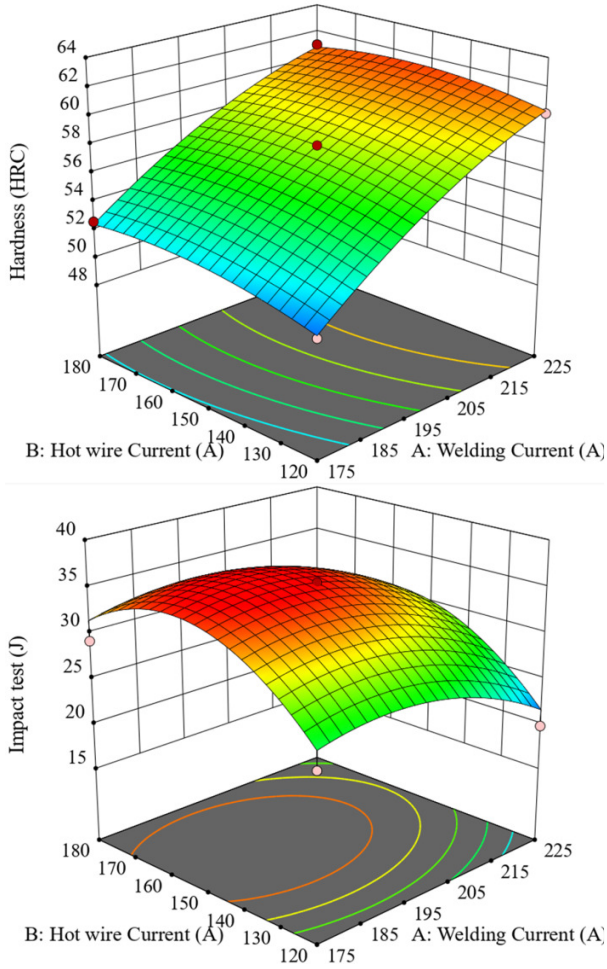

Fig. 4. RSM response surfaces of hardness and impact energy.

B. ANN-Based Prediction and Model Validation

ANN predictions were validated against experimental data and quadratic RSM–CCD models. The second–order RSM–CCD equations for HRC and IM as functions of WC and HWC are given in (9) and (10), following standard CCD formulations [11]. ANN surrogate modeling is recognized for capturing nonlinear welding responses under limited datasets [10]:

$$HRC = 77.17 - 0.9(WC) - 0.349(HWC) + 1.68 \times 10 - 3(WC)2 - 3.33x10 - 4(WC \cdot HWC) + 8.89x10 - 4(HWC)^2 \quad (9)$$

$$IM = 282.07 - 1.744(WC) - 1.932(HWC) + 4.71x10 - 3(WC)2 - 3.67\,x10 - 4(WC \cdot HWC) \quad (10)$$

Table VI summarizes the validation results and prediction accuracy. The ANN shows excellent agreement with experiments for both HRC (R^2 = 0.97, RMSE = 0.93) and IM (R^2 = 0.99, RMSE = 0.10), whereas the quadratic RSM–CCD yields acceptable accuracy for hardness (R^2 = 0.86) but limited performance for impact energy. This reflects the reduced capability of quadratic RSM to capture strong nonlinearity and variability in toughness-related responses, consistent with previous reports favoring ANN-based models for such conditions [12].

The run-by-run comparison in Figure 5 demonstrates that ANN predictions closely follow the experimental trends across all CCD runs, whereas the RSM–CCD model exhibits larger deviations, particularly for impact energy [10, 12]. This confirms that ANN is a more efficient surrogate predictor, justifying its use as the GA fitness function for multi-objective optimization, consistent with prior welding optimization studies [13].

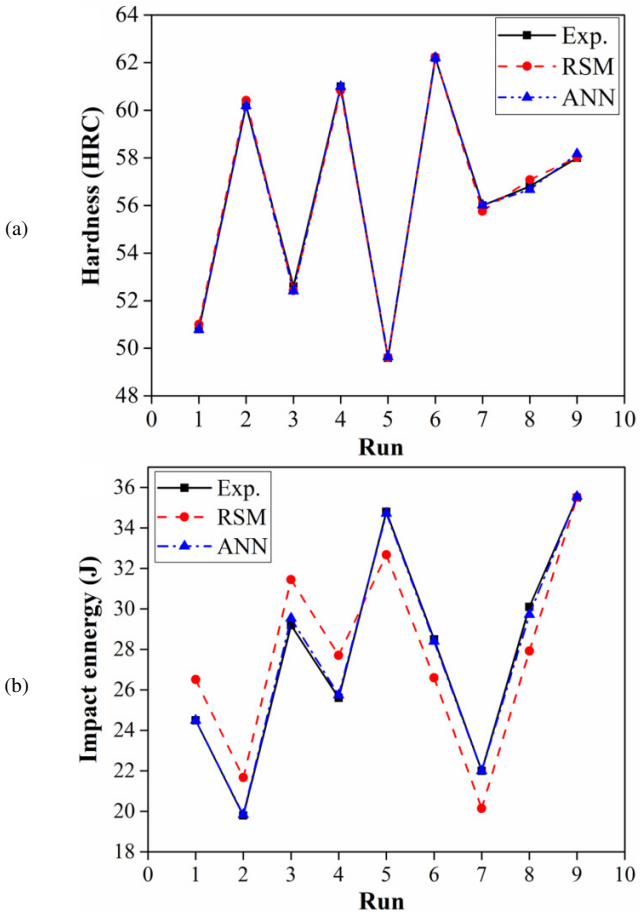

Fig. 5. Comparison of experimental and predicted responses.

C. ANN–GA Multi-Objective Optimization Results

Multi-objective optimization of TIG hot-wire welding parameters was conducted using a GA coupled with the trained ANN surrogate, where the ANN served as the fitness function to maximize hardness and impact energy via an overall desirability index [14]. The ANN–GA converged to a balanced condition that optimizes the strength–toughness trade-off [15]. The best and worst solutions are outlined in Table VII: the optimal setting (WC = 200 A, HWC = 150 A) yielded 58.17 HRC and 35.55 J with high desirability (D = 0.95, Rank 1), whereas a suboptimal condition (WC = 200 A, HWC = 107.57 A) produced 56.02 HRC and 22 J with low desirability (D = 0.43, Rank 9) [16]. These results highlight the significant role of HWC in controlling heat balance and impacting energy performance [17].

TABLE VII. BEST AND WORST ANN–GA WELDING SOLUTIONS

Case	WC	HWC	GA (HRC)	GA (J)	*D*	Rank
Optimal (best)	200	150	58.17	35.55	0.95	1
Non-optimal (worst)	200	107.57	56.02	22	0.43	9

Figure 6(a) demonstrates that HWC contributes more than WC to the optimal solution, complying with the role of hot-wire assistance in stabilizing melting and improving thermal control [18]. The convergence trends in Figure 6(b) indicate stable GA behavior, with rapid early improvement of best fitness and steady enhancement of mean fitness over 1000 generations, confirming efficient optimization performance [19]. These results validate the effectiveness of the ANN–GA framework in enhancing both hardness and impact energy under limited experimental data [10].

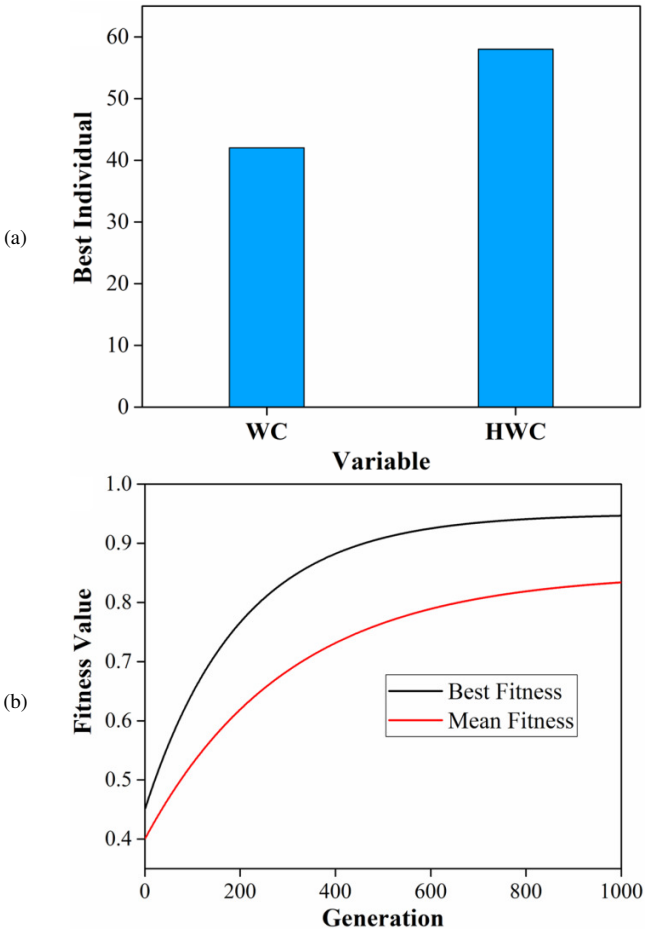

Fig. 6. ANN–GA convergence characteristics.

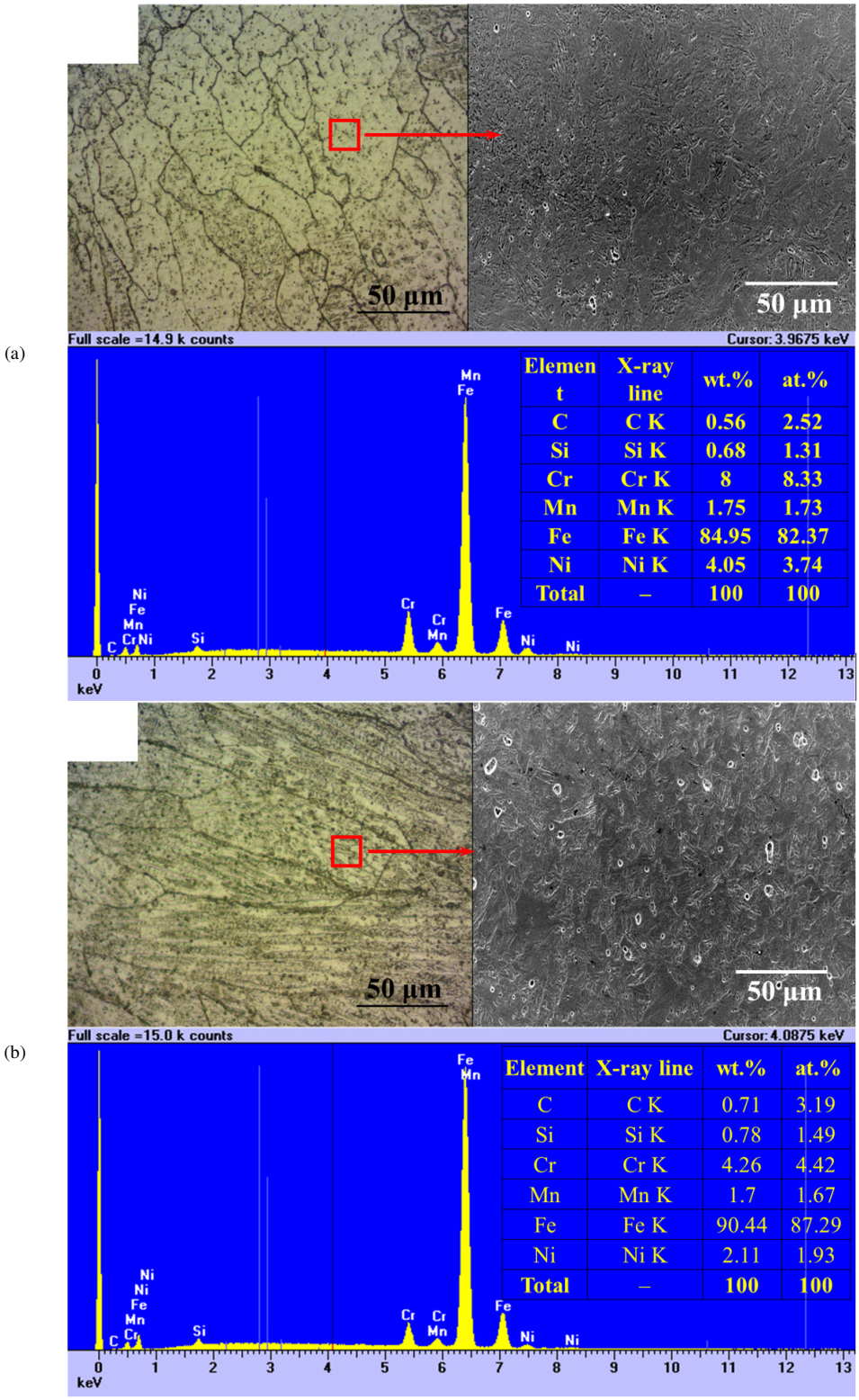

Fig. 7. Optical Microscopy-Scanning Electron Microscopy-Energy Dispersive Spectroscopy (OM–SEM–EDS) comparison of weld microstructures under: (a) optimal condition, (b) non-optimal condition.

D. Microstructural and Fracture Surface Analysis

Figure 7 compares weld-region microstructures and elemental distributions under ANN–GA-identified optimal and non-optimal TIG hot-wire conditions. The optimal case shows a more homogeneous OM etching and uniform SEM contrast, indicating stable heat input and consistent fusion–solidification behavior [20]. In hot-wire GTAW, filler-wire preheating enhances deposition efficiency and moderates thermal gradients, promoting controlled weld pool dynamics and reduced microstructural heterogeneity [21].

EDS analysis further supports this trend: the optimal condition exhibits higher Cr and Ni contents (≈8 wt.% Cr, ≈4 wt.% Ni) than the non-optimal case (≈4.3 wt.% Cr, ≈2.1 wt.% Ni), indicating enhanced alloying contribution and more stable elemental mixing in the weld pool [22]. Weld-metal composition, particularly the balance between ferrite and austenite stabilizers, governs impact toughness by controlling phase transformations, grain boundary characteristics, and the formation of brittle secondary phases [23].

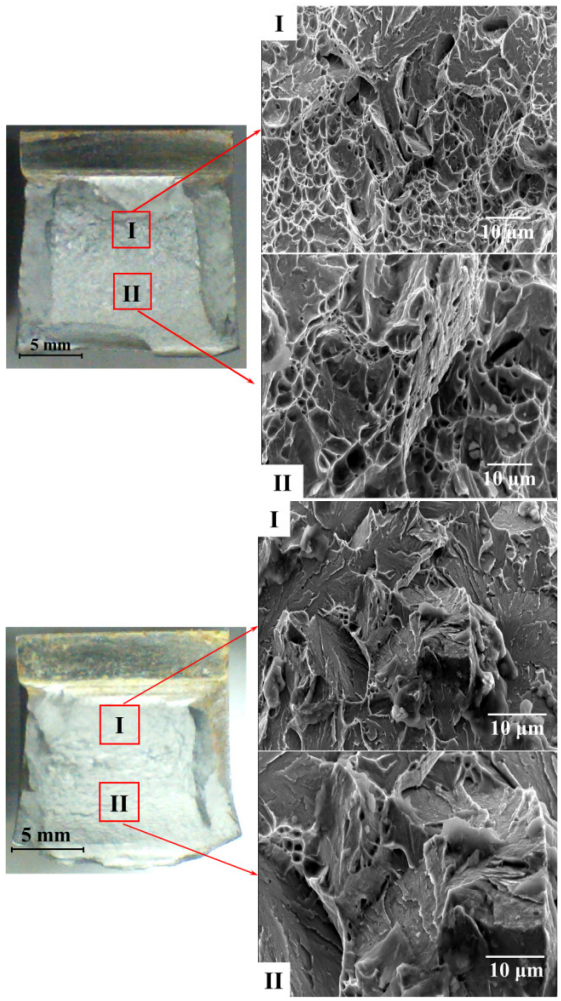

Fig. 8. Macro-fracture and SEM fractography of Charpy specimens for: (a) optimal, (b) non-optimal weld conditions.

Figure 8 shows macro-fracture surfaces and SEM fractography (Regions I–II) of Charpy specimens. The optimal weld exhibits ductile-dominant features with dense, deep dimples and extensive microvoid coalescence, indicating higher plastic deformation and impact energy [24]. In contrast, the non-optimal weld shows mixed-to-brittle characteristics, including quasi-cleavage facets and shallow dimples, consistent with reduced ductility [25]. These observations confirm that hot-wire-assisted heat balance promotes tougher fracture behavior, whereas unfavorable parameters induce local brittle zones that facilitate crack initiation under impact loading [26].

IV. CONCLUSION

This study developed a hybrid Response Surface Methodology–Artificial Neural Network–Genetic Algorithm (RSM–ANN–GA) framework for multi-response optimization of TIG hot-wire repair welding of AISI 5160, achieving simultaneous improvement in hardness and impact energy under a limited dataset. A compact nine-run Central Composite Design (CCD) effectively captured the design space, revealing a hardness of 49.6–62.2 HRC and an impact energy of 19.8–35.5 J, with a clear strength–toughness trade-off governed by heat input balance. RSM analysis indicated that hardness is mainly influenced by Welding Current (WC) and its quadratic term, while impact energy is dominated by Hot-Wire Current (HWC) and its nonlinear effect. The ANN model outperformed RSM with high accuracy (R^2 = 0.97 and 0.99) and low prediction errors, effectively capturing nonlinear relationships. Coupling ANN with GA enabled efficient optimization, yielding an optimal condition at WC = 200 A and HWC = 150 A, with 58.17 HRC and 35.55 J, with a high desirability (D) of 0.95, supported by improved ductile fracture characteristics. However, the limited dataset restricts statistical robustness; future work should expand experiments and validate results under service conditions, including fatigue and wear, while incorporating additional process variables.

DECLARATION OF COMPETING INTERESTS

The authors declare that they have no competing financial or non-financial interests that could have influenced the findings reported in this study.

ACKNOWLEDGMENT

This research received no external funding. The authors gratefully acknowledge the technical support provided by the laboratory staff of Nakhon Phanom University and Rajamangala University of Technology Suvarnabhumi during the experimental investigations.

DATA AVAILABILITY

The data supporting the findings of this study are entirely available within the article. Any additional information can be obtained from the corresponding author upon reasonable request.

AI USE AND DECLARATION OF GENERATIVE AI USE

During the preparation of this manuscript, the authors used ChatGPT solely for language editing and text refinement. The AI tool was not used for data analysis, modeling, or the

generation of scientific results. All content was critically reviewed and revised by the authors, who take full responsibility for the accuracy and integrity of the work.

REFERENCES

[1] X. Han, Z. Zhang, J. Hou, G. C. Barber, and F. Qiu, "Tribological Behavior of Shot Peened/Austempered AISI 5160 Steel," *Tribology International*, vol. 145, May 2020, Art. no. 106197, https://doi.org/10.1016/j.triboint.2020.106197.

[2] A. S. J. Jilabi, "A Comparative Study Between Oxy-Acetylene and Shielded Metal Arc Welds of AISI 5160 Low Alloy Steel," *Revue Des Composites et Des Matériaux Avancés*, vol. 34, no. 4, pp. 427–434, Aug. 2024, https://doi.org/10.18280/rcma.340404.

[3] P. Apichai, "Effects of Quenchants on Microstructures and Mechanical Properties of Steel Grade AISI 5160," *Journal of Metals, Materials and Minerals*, vol. 30, no. 3, Sep. 2020, https://doi.org/10.55713/jmmm.v30i3.631.

[4] H. E. Jaramillo S, N. A. De Sánchez, and J. A. Avila D, "Effect of the Shot Peening Process on the Fatigue Strength of SAE 5160 Steel," *Proceedings of the Institution of Mechanical Engineers, Part C: Journal of Mechanical Engineering Science*, vol. 233, no. 12, pp. 4328–4335, Jun. 2019, https://doi.org/10.1177/0954406218816349.

[5] Syafrizal, A. Akhyar, M. Iqbal, and Syukran, "Selection of Optimal Filler Metal for Dissimilar Welding of SA335 Gr. P11 and Incoloy 800 in Primary Reformer Tube Catalyst Repairs," *Engineering, Technology & Applied Science Research*, vol. 15, no. 6, pp. 29887–29893, Dec. 2025, https://doi.org/10.48084/etasr.14269.

[6] Tanmay, M. Chandra, S. Sharma, and S. S. Panda, "Study of Mechanical and Metallurgical Properties of Cold and Hot Reciprocating Wire TIG Welding on AISI 1035 Carbon Steel," *Journal of The Institution of Engineers (India): Series D*, vol. 102, no. 1, pp. 159–166, Jun. 2021, https://doi.org/10.1007/s40033-021-00249-2.

[7] A. Megalingam, A. H. Ahmad, N. A. Alang, J. Alias, and N. A. A. Razak, "Application of Response Surface Methodology for Parameter Optimization of Aluminum 7075 Thixoforming Feedstock Billet Production," *Journal of Materials Engineering and Performance*, vol. 32, no. 13, pp. 5919–5931, Jul. 2023, https://doi.org/10.1007/s11665-022-07535-4.

[8] I. Owunna and A. E. Ikpe, "Modelling and Prediction of the Mechanical Properties of TIG Welded Joint for AISI 4130 Low Carbon Steel Plates Using Artificial Neural Network (ANN) Approach," *Nigerian Journal of Technology*, vol. 38, no. 1, Jan. 2019, Art. no. 117, https://doi.org/10.4314/njt.v38i1.16.

[9] D. Kim, S. Rhee, and H. Park, "Modelling and Optimization of a GMA Welding Process by Genetic Algorithm and Response Surface Methodology," *International Journal of Production Research*, vol. 40, no. 7, pp. 1699–1711, Jan. 2002, https://doi.org/10.1080/00207540110119964.

[10] A. Mayai, S. Prasomthong, and Y. Pookamnerd, "Development of Hybrid ANN-GA and RSM Models for Optimizing Mechanical Properties in SS400-SUS304 Welds," *EUREKA: Physics and Engineering*, no. 3, pp. 152–165, May 2025, https://doi.org/10.21303/2461-4262.2025.003606.

[11] A. Silachai and S. Prasomthong, "Optimized Parameter of Dissimilar Joining Between Al6061-T6 and Height-Strength Steel with Friction Stir Spot Welding Process (FSSW)," *Journal of Metals, Materials and Minerals*, vol. 32, no. 4, pp. 118–127, Dec. 2022, https://doi.org/10.55713/jmmm.v32i4.1538.

[12] M. A. Alam *et al.*, "Modelling and Optimisation of Hardness Behaviour of Sintered Al/SiC Composites Using RSM and ANN: A Comparative Study," *Journal of Materials Research and Technology*, vol. 9, no. 6, pp. 14036–14050, Nov. 2020, https://doi.org/10.1016/j.jmrt.2020.09.087.

[13] P. G. Mongan *et al.*, "Multi-Objective Optimisation of Ultrasonically Welded Dissimilar Joints Through Machine Learning," *Journal of Intelligent Manufacturing*, vol. 33, no. 4, pp. 1125–1138, Apr. 2022, https://doi.org/10.1007/s10845-022-01911-6.

[14] I. D. V. Tomaz, F. H. G. Colaço, S. Sarfraz, D. Yu. Pimenov, M. K. Gupta, and G. Pintaude, "Investigations on Quality Characteristics in Gas Tungsten Arc Welding Process Using Artificial Neural Network Integrated with Genetic Algorithm," *The International Journal of Advanced Manufacturing Technology*, vol. 113, no. 11–12, pp. 3569–3583, Apr. 2021, https://doi.org/10.1007/s00170-021-06846-5.

[15] A. K. Mengistie and T. M. Bogale, "Development of Automatic Orbital Pipe MIG Welding System and Process Parameters' Optimization of AISI 1020 Mild Steel Pipe Using Hybrid Artificial Neural Network and Genetic Algorithm," *The International Journal of Advanced Manufacturing Technology*, vol. 128, no. 5–6, pp. 2013–2028, Sep. 2023, https://doi.org/10.1007/s00170-023-11796-1.

[16] T. Medhi, S. A. I. Hussain, B. S. Roy, and S. C. Saha, "An Intelligent Multi-Objective Framework for Optimizing Friction-Stir Welding Process Parameters," *Applied Soft Computing*, vol. 104, Jun. 2021, Art. no. 107190, https://doi.org/10.1016/j.asoc.2021.107190.

[17] N. Suwannatee, M. Yamamoto, and S. Shinohara, "Optimization of Hot-Wire Fraction for Enhance Quality in GMAW," *Welding in the World*, vol. 68, no. 5, pp. 1017–1032, May 2024, https://doi.org/10.1007/s40194-023-01623-2.

[18] V. Poonguzhali, T. Deepan Bharathi Kannan, M. Umar, and P. Sathiya, "Application of ANN Modelling and GA Optimization for Improved Creep and Corrosion Properties of Spin-Arc Welded AA5083-H111 Alloy," *Russian Journal of Non-Ferrous Metals*, vol. 61, no. 2, pp. 188–198, Mar. 2020, https://doi.org/10.3103/S1067821220020091.

[19] K. Kamal Babu *et al.*, "Parameter Optimization of Friction Stir Welding of Cryorolled AA2219 Alloy Using Artificial Neural Network Modeling with Genetic Algorithm," *The International Journal of Advanced Manufacturing Technology*, vol. 94, no. 9–12, pp. 3117–3129, Feb. 2018, https://doi.org/10.1007/s00170-017-0897-6.

[20] R. Darji, V. Badheka, K. Mehta, J. Joshi, A. Yadav, and A. K. Chakraborty, "Investigation on Stability of Weld Morphology, Microstructure of Processed Zones, and Weld Quality Assessment for Hot Wire Gas Tungsten Arc Welding of Electrolytic Tough Pitch Copper," *Materials and Manufacturing Processes*, vol. 37, no. 8, pp. 908–920, Jun. 2022, https://doi.org/10.1080/10426914.2021.1981931.

[21] T. Ungethüm, P. Schilling, E. Spaniol, and U. Füssel, "GMAW Hot-Wire Process with Indirect Resistive Heating of the Auxiliary Wire," *Welding in the World*, vol. 67, no. 8, pp. 2031–2038, Aug. 2023, https://doi.org/10.1007/s40194-023-01529-z.

[22] M. Abbasi, B. B. Vanani, A. Tahaei, and G. L. Garagnani, "Influence of Ni and PWHT on Microstructure Evolution and Mechanical Properties of GTA-Welded Duplex Stainless Steel and Super Duplex Stainless Steel Joints: A Comparative Investigation," *Proceedings of the Institution of Mechanical Engineers, Part L: Journal of Materials: Design and Applications*, vol. 238, no. 10, pp. 1914–1928, Oct. 2024, https://doi.org/10.1177/14644207241236743.

[23] V. Balaguru, V. Balasubramanian, and P. Sivakumar, "Effect of Weld Metal Composition on Impact Toughness Properties of Shielded Metal Arc Welded Ultra-High Hard Armor Steel Joints," *Journal of the Mechanical Behavior of Materials*, vol. 29, no. 1, pp. 186–194, Dec. 2020, https://doi.org/10.1515/jmbm-2020-0019.

[24] R. Prokić Cvetković, O. Popović, L. Radović, A. Sedmak, and I. Cvetković, "Fracture Behavior of AlMg4.5Mn Weld Metal at Different Temperatures under Impact Loading," *Sustainability*, vol. 15, no. 2, Jan. 2023, Art. no. 1550, https://doi.org/10.3390/su15021550.

[25] A. Takahashi, T. Toyohiro, Y. Segawa, M. Kobayashi, and H. Miura, "Embrittlement Fracture Behavior and Mechanical Properties in Heat-Affected Zone of Welded Maraging Steel," *Materials*, vol. 17, no. 2, Jan. 2024, Art. no. 440, https://doi.org/10.3390/ma17020440.

[26] J. Li *et al.*, "Influence of Heat Input on the Microstructure and Impact Toughness in Weld Metal by High-Efficiency Submerged Arc Welding," *Metals*, vol. 13, no. 7, Jun. 2023, Art. no. 1217, https://doi.org/10.3390/met13071217.